

Light by Light Scattering as a New Probe for Axions

Soroush Shakeri,^{1,2,3,*} David J. E. Marsh,^{4,†} and She-Sheng Xue^{5,6,‡}

¹*Department of Physics, Isfahan University of Technology, Isfahan 84156-83111, Iran*

²*ICRANet-Isfahan, Isfahan University of Technology, 84156-83111, Iran*

³*Institute for Research in Fundamental Sciences (IPM), P. O. Box 19395-5531, Tehran, Iran*

⁴*Institut für Astrophysik, Georg-August Universität, Friedrich-Hund-Platz 1, D-37077 Göttingen, Germany*

⁵*ICRANet Piazzale della Repubblica, 10 -65122, Pescara, Italy*

⁶*Physics Department, University of Rome La Sapienza,*

P.le Aldo Moro 5, 100185 Rome, Italy

(Dated: February 17, 2020)

We study the impact of virtual axions on the polarization of photons inside a cavity during the interaction of high-power laser pulses. A novel detection scheme for measuring the axion-induced ellipticity signal during the Light-by-Light (LBL) scattering process is investigated. We show that a momentum exchange between photons in a probe laser beam and a high-intensity target beam may lead to a resonance at the physical mass of the axion. Consequently, the resonant enhancement of vacuum birefringence gives rise to a large ellipticity signal. This signal enhancement can be applied in order to discriminate between the axion contribution to LBL scattering and the standard model contribution due to electron-positron pairs. The sensitivity of the scheme is studied for experimentally feasible probe light sources and ultrahigh intensity laser backgrounds. It is shown that this technique has the potential to probe the QCD axion in the mass range $10^{-2}\text{eV} \lesssim m_a \lesssim 1\text{eV}$. In this region the axion induced signal surpasses the standard model background.

I. INTRODUCTION

Axions are hypothetical pseudo-scalar bosons originally proposed as part of the Peccei-Quinn (PQ) mechanism to explain the lack of CP violation in the strong interaction [1–4]. A more general class of Axion Like Particles (ALPs) naturally emerge in the low-energy effective theory of string compactifications [5, 6]. Hereafter we collectively call both the QCD axion and the ALP, "axion". Sufficiently light axions could also provide a broad class of well-motivated Dark Matter (DM) candidates [7–9]. Research into the detectability of axions has recently revealed a vast number of promising experimental designs. As yet, however, there is no experimental evidence of the existence of axions.

Axions can couple to two photons and this property allows one to design high-precision optical setups to detect them. Photons can mix with axions in the presence of external magnetic field, which underlies the design of dark matter "haloscope" microwave cavities [10–14]. The impact of axions on photon polarization during photon propagation through an axion background also provides an effective detection strategy [15–19]. In the last decade laser technology and high-precision optical components have been applied as an effective way to probe axions. So far several polarimetric experiments such as BRFT [20], PVLAS [21], BMV [22] and Q&A [4] have been proposed in order to find indirect evidences of axions. These experiments are mainly based on measuring dichroism or birefringence properties induced by axion-photon interaction. It has been shown that axion field induces a birefringence and/or dichroism on a linearly polarized probe laser beam [23, 24].

Besides these efforts, elastic photon-photon scattering via virtual axion mediator may open new doors to look for axions [25–29]. Observational signal introduced by virtual axions do not rely on the nature of axion as DM. However elastic photon-photon scattering is also permitted in quantum electrodynamics (QED) framework owing to the photon interaction with virtual electron-positron pairs [30–34]. Therefore it is essential task to realize axion fingerprints in the presence of an irreducible background comes from standard QED processes.

Looking for resonances in the cross section of light-by-light (LBL) scattering is a possible way to search for (relatively) heavy axions [35, 36] at particle colliders. Recently, measurement of LBL scattering in ultra-peripheral heavy-ion collisions was reported by the ATLAS collaboration [37], where the results are in agreement with QED predictions [38, 39]. Soon after this detection the corresponding bounds on the axion-photon coupling were reported in [35, 40] and more recently in [41] especially for resonant production of axions.

High-power laser facilities are complementary to colliders to detect LBL scattering as a manifestation of vacuum nonlinearities. The present article presents a novel method to detect axions based on their polarization signal in high intensity laser-laser

*s.shakeri@iut.ac.ir

†david.marsh@uni-goettingen.de

‡xue@icra.it

collisions. Due to the pseudo-scalar nature of the axion-photon coupling, the axion field generates polarization asymmetry between left- and right-handed circularly polarized photons. Hence a net circular polarized emission arises as an indication to mediating axions in LBL scattering event.

The potential of such experiments to detect axions by measuring vacuum birefringence has so far been examined in [42, 43], where the classical equation of motion for a system of EM fields and axions was considered. Previous investigations have mainly relied on the perturbative solution of the classical field equations, in the presence of a constant magnetic field, in order to find the evolution of the propagating polarization modes. In contrast to the previous studies, our quantum mechanical treatment respects to the quantum structure of photons and axions which reveals more details about the photon-photon scattering process with axions in the intermediate state. Our approach is based on a quantum-mechanical description of the Stokes parameters and their time evolution, given by the quantum Boltzmann equation [44].

Recently, we have proposed a novel detection method based on the forward scattering of photons via virtual axion exchange from an inhomogeneous magnetic field inside a cavity [45]. It has been shown that a momentum exchange between the cavity photons and the non-uniform magnetic field causes a resonance enhancement of the birefringence signal, this has the potential to probe a broad range of axion mass. In the present paper we propose a new setup in which the background magnetic field is replaced by an ultrahigh intensity laser such as many petawatt class lasers already exist. We consider the generation of elliptical polarization for an initially linearly polarized probe laser beam interacting with a high power laser which is pumped into a tunable cavity. Thanks to the resonance pole in the s-channel axion propagator of photon-photon scattering, one can explore a wide range of axion mass with a variable frequency light source.

A similar polarization signal in the standard model is generated by QED processes [44, 46, 47]. It is highly desirable to find a proper setup to separate the vacuum birefringence effects as predicted by QED and those induced by virtual axions. Taking the quantum Boltzmann equation as our theoretical framework, we discuss both the contribution of axions and QED to the predicted signal. We show that it is possible to scan a considerable axions mass range $10^{-2}\text{eV} \lesssim m_a \lesssim 1\text{eV}$ by measuring elliptical polarization generated on resonance, where the effect of axions and QED can be distinguished.

This paper is organized as follows. In section II, we discuss the evolution of photon polarization in photon-photon scattering process owing to the axion-photon interaction and the nonlinear Euler-Heisenberg interaction. In Section III, we consider the generation of circular polarization in terms of the ellipticity parameter as an observable quantity in laser-laser collision experiments. This section ends by deriving the potential reach of this technique on axion parameter space. Finally, we conclude in section IV.

II. PHOTON POLARIZATION AND PHOTON-PHOTON SCATTERING

In the standard model, the lowest order photon-photon scattering occurs at one loop via virtual electron-positron pairs. In axion electrodynamics, however, virtual axions lead to the same process at the level. The polarized virtual electron-positron pairs cause nonlinear interaction of EM fields when the QED vacuum is exposed to intense light. The nonlinear interaction of EM fields with equivalent photon energies much less than electron mass ($\omega \ll m_e$) can be well approximated by the effective Euler-Heisenberg (EH) Lagrangian [30–34]. The EH lagrangian can be obtained by integrating out the fermionic degrees of freedom, and at one-loop is given by

$$\mathcal{L}_{int}^{EH} = \frac{\alpha^2}{90m_e^4} \left[(\mathcal{F}_{\mu\nu}\mathcal{F}^{\mu\nu})^2 + \frac{7}{4}(\mathcal{F}_{\mu\nu}\tilde{\mathcal{F}}^{\mu\nu})^2 \right], \quad (1)$$

where α is the fine-structure constant, m_e is the electron mass, $\mathcal{F}_{\mu\nu}$ is the EM field strength tensor and $\tilde{\mathcal{F}}^{\mu\nu} \equiv \varepsilon^{\mu\nu\rho\sigma}\mathcal{F}_{\rho\sigma}$. The field strength tensor $\mathcal{F}_{\mu\nu} = \partial_\mu\mathcal{A}_\nu - \partial_\nu\mathcal{A}_\mu$ can be expressed in terms of the quantum gauge field \mathcal{A}_μ as a linear combination of creation and annihilation operators

$$\mathcal{A}_\mu(x) = \int \frac{d^3k}{(2\pi)^3 2k^0} \sum_{i=1,2} \left[a_i(\mathbf{k})\varepsilon_{i\mu}(\mathbf{k})e^{-ik\cdot x} + a_i^\dagger(\mathbf{k})\varepsilon_{i\mu}^*(\mathbf{k})e^{ik\cdot x} \right], \quad (2)$$

where $\varepsilon_{i\mu}(\mathbf{k}) = (0, \vec{\varepsilon}_i(\mathbf{k}))$ shows the photon polarization four-vector for the two orthogonal transverse polarizations and k (with $k^0 = |\mathbf{k}|$) stands for the four-momentum vector. Meanwhile $a_i^\dagger(\mathbf{k})$ and $a_i(\mathbf{k})$ satisfy the common canonical commutation relation as

$$\left[a_i(\mathbf{k}), a_j^\dagger(\mathbf{k}') \right] = (2\pi)^3 2k^0 \delta_{ij} \delta^{(3)}(\mathbf{k} - \mathbf{k}'). \quad (3)$$

On the other hand, the axion-photon-photon vertex leads to photon-photon scattering mediated by virtual axions. The axion-photon interaction is described by the Lagrangian [1–3]

$$\mathcal{L}_{int}^{a\gamma\gamma} = -\frac{g_{a\gamma\gamma}}{4} a \mathcal{F}_{\mu\nu} \tilde{\mathcal{F}}^{\mu\nu}, \quad (4)$$

where $g_{a\gamma\gamma}$ is the coupling constant, and a is the pseudoscalar axion field. In a similar procedure of constructing the effective EH Lagrangian (1), axions with masses larger than the typical energy of scattered photons ($m_a \gg \omega$) can be integrated out giving rise to an effective interaction term [28, 29],

$$\mathcal{L}_{int}^{\text{eff},a} = \frac{g_{a\gamma\gamma}^2}{32m_a^2} (\mathcal{F}_{\mu\nu} \tilde{\mathcal{F}}^{\mu\nu})^2. \quad (5)$$

In the following, we focus on the polarization characteristics induced on an EM beam through light by light scattering. The polarization properties of an EM wave are usually described in terms of the Stokes parameters: the total intensity I , linear polarization Q and U , and the circular polarization V . In a quantum-mechanical description of light polarization [48, 49], a given photon state $|\mathcal{A}\rangle$ can be expanded in the polarization basis as

$$|\mathcal{A}\rangle = \sum_i a_i |\varepsilon_i\rangle, \quad (6)$$

where $|\varepsilon_i\rangle$ defines the polarization states and a_i corresponds to the amplitude of different components. Moreover the Stokes operators, in the linear basis associated to each Stokes parameter, are given by

$$\hat{I} = |\varepsilon_1\rangle\langle\varepsilon_1| + |\varepsilon_2\rangle\langle\varepsilon_2|, \quad (7)$$

$$\hat{Q} = |\varepsilon_1\rangle\langle\varepsilon_1| - |\varepsilon_2\rangle\langle\varepsilon_2|, \quad (8)$$

$$\hat{U} = |\varepsilon_1\rangle\langle\varepsilon_2| + |\varepsilon_2\rangle\langle\varepsilon_1|, \quad (9)$$

$$\hat{V} = i|\varepsilon_2\rangle\langle\varepsilon_1| - i|\varepsilon_1\rangle\langle\varepsilon_2|. \quad (10)$$

In a general mixed state of photons, a normalized density matrix $\rho_{ij} \equiv (|\varepsilon_i\rangle\langle\varepsilon_j|/\text{tr}\rho)$ describes an ensemble of photons [50]. The expectation values of the Stokes operators reproduce the classical Stokes parameters as

$$I \equiv \langle\hat{I}\rangle = \text{tr}\rho\hat{I} = \rho_{11} + \rho_{22}, \quad (11)$$

$$Q \equiv \langle\hat{Q}\rangle = \text{tr}\rho\hat{Q} = \rho_{11} - \rho_{22}, \quad (12)$$

$$U \equiv \langle\hat{U}\rangle = \text{tr}\rho\hat{U} = \rho_{12} + \rho_{21}, \quad (13)$$

$$V \equiv \langle\hat{V}\rangle = \text{tr}\rho\hat{V} = i(\rho_{12} - \rho_{21}). \quad (14)$$

These relations show how polarization information is encoded in the density matrix, the explicit representation of this matrix in terms of Stokes parameters is given by

$$\rho = \frac{1}{2} \begin{pmatrix} I+Q & U-iV \\ U+iV & I-Q \end{pmatrix}. \quad (15)$$

The time evolution of the density matrix, and hence the time evolution of Stokes parameters, is obtained from the quantum Boltzmann equation [48, 49]

$$(2\pi)^3 2k^0 \delta^{(3)}(0) \frac{d}{dt} \rho_{ij}(\mathbf{k}) = i \langle [\hat{\mathcal{H}}_{int}(t), \hat{D}_{ij}(\mathbf{k})] \rangle - \frac{1}{2} \int_{-\infty}^{+\infty} dt \langle [\hat{\mathcal{H}}_{int}(t), [\hat{\mathcal{H}}_{int}(0), \hat{D}_{ij}(\mathbf{k})]] \rangle, \quad (16)$$

where $\hat{\mathcal{H}}_{int}$ is the first order interaction Hamiltonian and $D_{ij}^0(\mathbf{k}) \equiv a_i^\dagger(\mathbf{k})a_j(\mathbf{k})$ is the photon number operator. The first term on the right-hand side of Eq. (16) is the forward-scattering term describing only the variation of the photon polarization, the second term is due to higher order collision terms corresponding to the scattering processes. In the following, we will adopt interaction terms Eqs. (4) and (1) in order to compute the time-evolution of the density matrix.

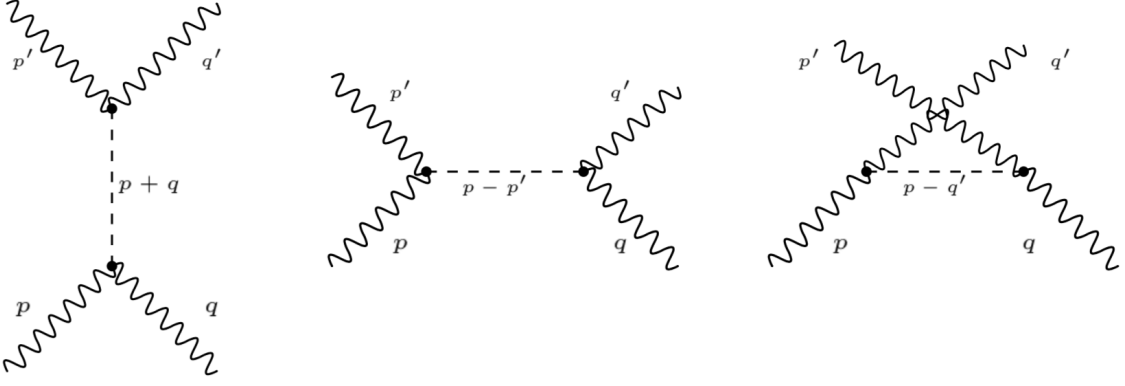


FIG. 1: Photon-Photon scattering via axion exchange in the different scattering channels s,t and u from left to right, respectively.

A. Circular Polarization Due to Photon-Axion Interactions

The two-photon-axion interaction Eq. (4) allows for axion decay into two photons ($a \rightarrow \gamma\gamma$) where the decay rate is given by [51, 52]

$$\Gamma_{a \rightarrow \gamma\gamma} = \frac{g_{a\gamma\gamma}^2 m_a^3}{64\pi}, \quad (17)$$

this quantity is strongly suppressed for very low mass axions, implying that the axion is stable on cosmic time scales (and hence it is a dark matter candidate). Due to the long lifetime, axion-photon conversion $a \rightarrow \gamma$ is usually considered in the presence of external sources of EM fields [53, 54].

Due to its interaction with quarks and gluons, and the presence of QCD instantons, the QCD axion obtains a mass below the QCD scale [55, 56]:

$$m_a = \frac{f_\pi m_\pi}{f_a} \frac{\sqrt{z}}{1+z} \approx 6eV \left(\frac{10^6 GeV}{f_a} \right) \quad (18)$$

where f_a is the axion decay constant (the scale of spontaneous symmetry breaking, of which the axion is a pseudo-Goldstone boson), $f_\pi = 93$ MeV and $m_\pi = 135$ MeV are the pion decay constant and pion mass, respectively, and $z = m_u/m_d$ is the mass ratio of up and down quarks [57]. The axion-photon coupling $g_{a\gamma\gamma}$ can be expressed in terms of the axion decay constant as

$$g_{\gamma\gamma a} = \frac{\alpha C}{2\pi f_a} \quad (19)$$

where C is a dimensionless, model dependent parameter, with contributions from both the colour and electromagnetic anomaly (see e.g. Ref. [58]). Taking the C to be of order unity as in the conventional QCD axion models [59–62] and using Eqs. (18) and (19), the axion decay rate Eq. (17) is:

$$\Gamma_{a \rightarrow \gamma\gamma} \simeq 3 \times 10^{-25} \left(\frac{m_a}{eV} \right)^5 s^{-1}. \quad (20)$$

Therefore, QCD axions with $m_a < 18eV$ live longer than the age of the universe [63].

Taking into account the finite lifetime, the Fourier transform of the propagator is

$$i\Delta_a(x) = \frac{1}{(2\pi)^4} \int d^4k \frac{i}{k^2 - m_a^2 + im_a\Gamma} e^{-ik \cdot x}, \quad (21)$$

where Γ is the total decay width of the axion $\Gamma \geq \Gamma_{a \rightarrow \gamma\gamma}$. The decay width can be parametrized by the branching ratio into photons as $\mathcal{B}_{a \rightarrow \gamma\gamma} = \Gamma_{a \rightarrow \gamma\gamma}/\Gamma$. We consider only axion masses below $2m_e$ where axions can only decay into photons (the axion has no coupling to neutrinos in the canonical models) and therefore we set $\mathcal{B}_{a \rightarrow \gamma\gamma} = 1$ in our computations [64].

Considering the axion-photon interaction Eq. (4), the Fourier transformations of photon field Eq. (2) and axion propagator Eq. (21), the Hamiltonian describing the axion-photon-photon interaction is:

$$\begin{aligned} \mathcal{H}_{int}^{\gamma\gamma}(t) = & g_{a\gamma\gamma}^2 \int d\mathbf{p} d\mathbf{q} d\mathbf{p}' d\mathbf{q}' (2\pi)^3 \delta^3(\mathbf{p} + \mathbf{q} - \mathbf{p}' - \mathbf{q}') e^{i(p_0+q_0-p'_0-q'_0)t} a_s^\dagger(\mathbf{p}') a_r^\dagger(\mathbf{q}') \left[\frac{A}{(p+q)^2 - m_a^2 + im_a\Gamma} \right. \\ & \left. + \frac{B}{(p-p')^2 - m_a^2 + im_a\Gamma} + \frac{C}{(p-q')^2 - m_a^2 + im_a\Gamma} \right] a_s(p) a_r(q), \end{aligned} \quad (22)$$

where $d\mathbf{p} = \frac{d^3\mathbf{p}}{(2\pi)^3 2p_0}$, and similarly for \mathbf{p}' , \mathbf{q} and \mathbf{q}' . Coefficients A , B and C contain the information about the Lorentz and polarization structure which are related to different scattering channels s , t , u respectively, and are given by:

$$A = \varepsilon^{\mu\nu\alpha\beta} \varepsilon^{\mu'\nu'\alpha'\beta'} p_\mu \varepsilon_{s\nu}(\mathbf{p}) q_\alpha \varepsilon_{r\beta}(\mathbf{q}) p'_{\mu'} \varepsilon_{s'\nu'}(\mathbf{p}') q'_{\alpha'} \varepsilon_{r'\beta'}(\mathbf{q}'), \quad (23)$$

$$B = \varepsilon^{\mu\nu\alpha\beta} \varepsilon^{\mu'\nu'\alpha'\beta'} p_\mu \varepsilon_{s\nu}(\mathbf{p}) p'_{\alpha'} \varepsilon_{s'\beta}(\mathbf{p}') q_{\mu'} \varepsilon_{r\nu'}(\mathbf{q}) q'_{\alpha'} \varepsilon_{r'\beta'}(\mathbf{q}'), \quad (24)$$

$$C = \varepsilon^{\mu\nu\alpha\beta} \varepsilon^{\mu'\nu'\alpha'\beta'} p_\mu \varepsilon_{s\nu}(\mathbf{p}) q'_{\alpha'} \varepsilon_{r'\beta}(\mathbf{q}') p'_{\mu'} \varepsilon_{s'\nu'}(\mathbf{p}') q_{\alpha'} \varepsilon_{r\beta}(\mathbf{q}). \quad (25)$$

The corresponding Feynman diagrams of photon-photon scattering by an axion mediator in the different scattering channels are presented in Fig (1).

In the following we adopt the interaction Hamiltonian Eq. (22) in order to evaluate the time-evolution of the density matrix. We only focus on the leading term (forward-scattering) in the Boltzmann equation Eq. (16). In the forward scattering process, the momentum of photons does not change during interaction, and hence $\mathbf{p} = \mathbf{p}'$ and $\mathbf{q} = \mathbf{q}' = \mathbf{k}$. We substitute Eq. (22) into Eq. (16) and performing some straightforward computations using the following ensemble averages [44, 49]

$$\langle a_s^\dagger(\mathbf{p}) a_{s'}(\mathbf{q}) \rangle = 2p^0 (2\pi)^3 \delta^3(\mathbf{p} - \mathbf{q}) \rho_{ss'}(\mathbf{p}), \quad (26)$$

and

$$\begin{aligned} \langle a_{s'}^\dagger(\mathbf{p}') a_s(\mathbf{p}) a_{r'}^\dagger(\mathbf{q}') a_r(\mathbf{q}) \rangle &= 4q^0 p^0 (2\pi)^6 \delta^3(\mathbf{p} - \mathbf{p}') \delta^3(\mathbf{q} - \mathbf{q}') \rho_{ss'}(\mathbf{p}) \rho_{rr'}(\mathbf{q}) \\ &+ 4q^0 p^0 (2\pi)^6 \delta^3(\mathbf{p} - \mathbf{q}') \delta^3(\mathbf{q} - \mathbf{p}') \rho_{rs'}(\mathbf{q}) [\rho_{s'r'}(\mathbf{p}) + \delta_{s'r'}]. \end{aligned} \quad (27)$$

The time evolution of the photon density matrix $\dot{\rho}_{ij}^\gamma = \dot{\rho}_{ij}^{\gamma(\text{Axion})} + \dot{\rho}_{ij}^{\gamma(\text{QED})}$ contains contributions from the axion and QED terms. The axion contribution is given by

$$\begin{aligned} \dot{\rho}_{ij}(\mathbf{k})^{\gamma(\text{Axion})} &= \frac{2ig_a^2 \alpha \gamma \gamma}{k_0} \int \frac{d^3p}{(2\pi)^3 2p^0} \varepsilon^{\mu\nu\alpha\beta} \varepsilon^{\mu'\nu'\alpha'\beta'} p_\mu p_{\mu'} k_\alpha k_{\alpha'} \varepsilon_{s\nu}(p) \varepsilon_{s'\nu'}(p) \varepsilon_{r\beta}(k) \varepsilon_{r'\beta'}(k) \\ &\times \left[\frac{\rho_{rr'}(\mathbf{p})}{2p \cdot k - m_a^2 + im_a \Gamma} - \frac{\rho_{r'r}(\mathbf{p})}{2p \cdot k + m_a^2 + im_a \Gamma} \right] (\delta_{s'i} \rho_{sj}(\mathbf{k}) - \delta_{sj} \rho_{is'}(\mathbf{k})) \\ &= \frac{2ig_a^2 \alpha \gamma \gamma}{k_0} \int \frac{d^3p}{(2\pi)^3 2p^0} \varepsilon^{\mu\nu\alpha\beta} \varepsilon^{\mu'\nu'\alpha'\beta'} p_\mu p_{\mu'} k_\alpha k_{\alpha'} \varepsilon_{s\nu}(p) \varepsilon_{s'\nu'}(p) \varepsilon_{r\beta}(k) \varepsilon_{r'\beta'}(k) \\ &\times \left[\frac{m_a^2 (\rho_{rr'}(\mathbf{p}) + \rho_{r'r}(\mathbf{p})) + (2p \cdot k + im_a \Gamma) (\rho_{rr'}(\mathbf{p}) - \rho_{r'r}(\mathbf{p}))}{(2p \cdot k - m_a^2 + im_a \Gamma) (2p \cdot k + m_a^2 + im_a \Gamma)} \right] (\delta_{s'i} \rho_{sj}(\mathbf{k}) - \delta_{sj} \rho_{is'}(\mathbf{k})) + \mathcal{O}(g_a^4 \alpha \gamma \gamma). \end{aligned} \quad (28)$$

We will present $\dot{\rho}_{ij}^{\gamma(\text{QED})}$ in Sec. (II B).

In order to compute the effect of the axion interaction on photon polarization in light-by-light scattering in a realistic experimental setup with laser beams, we define $p_\alpha = p_0(1, \hat{\mathbf{p}})$, $k_\alpha = k_0(1, \hat{\mathbf{k}})$ and $\varepsilon_{\mu r} = (0, \hat{\varepsilon}_r)$, with $\hat{\mathbf{k}}$, $\hat{\varepsilon}_1(\mathbf{k})$, and $\hat{\varepsilon}_2(\mathbf{k})$ taken in the co-ordinates

$$\hat{\mathbf{k}} = \begin{pmatrix} 0 \\ 0 \\ 1 \end{pmatrix}, \quad \hat{\varepsilon}_1(\mathbf{k}) = \begin{pmatrix} 1 \\ 0 \\ 0 \end{pmatrix}, \quad \hat{\varepsilon}_2(\mathbf{k}) = \begin{pmatrix} 0 \\ 1 \\ 0 \end{pmatrix}, \quad (29)$$

and $\hat{\mathbf{p}}$, $\hat{\varepsilon}_1(\mathbf{p})$ and $\hat{\varepsilon}_2(\mathbf{p})$ are then

$$\hat{\mathbf{p}} = \begin{pmatrix} \sin \theta \cos \phi \\ \sin \theta \sin \phi \\ \cos \theta \end{pmatrix}, \quad \hat{\varepsilon}_1(\mathbf{p}) = \begin{pmatrix} \cos \theta \cos \phi \\ \cos \theta \sin \phi \\ -\sin \theta \end{pmatrix}, \quad \hat{\varepsilon}_2(\mathbf{p}) = \begin{pmatrix} -\sin \phi \\ \cos \phi \\ 0 \end{pmatrix}. \quad (30)$$

In the case of two approximately monochromatic laser beams, the density matrix can be represented as

$$\rho_{ij}(\mathbf{p}) \propto \delta^3(\mathbf{p} - \bar{\mathbf{p}}), \quad \rho_{ij}(\mathbf{k}) \propto \delta^3(\mathbf{k} - \bar{\mathbf{k}}), \quad (31)$$

where $\bar{\mathbf{k}}$ and $\bar{\mathbf{p}}$ stand for the mean momentum of the incident and target laser beams, respectively. As a result, the momentum integral over Stokes parameters can be replaced by the mean values of the corresponding quantities of the "target" laser beam. For instance, the mean value of $Q(\mathbf{p})$ is defined as

$$\int \frac{p^0 d^3 p}{(2\pi)^3} Q(\mathbf{p}) = \bar{Q}(\bar{\mathbf{p}}). \quad (32)$$

From now on, we assume that the target laser beam is totally linear polarized in the Q direction so $\bar{I}(\bar{\mathbf{p}}) = \bar{Q}(\bar{\mathbf{p}})$ where $\bar{I}(\bar{\mathbf{p}})$ is the mean intensity of the target laser beam. This means that the circular polarization $V(\bar{\mathbf{p}})$ of the target beam is assumed to be zero. Performing the momentum integration similar to Eq. (32), the time evolution of the Stokes parameters (as components of density matrix Eq. 15) due to photon-photon scattering by an axion mediator is given by

$$\dot{I} = 0, \quad \dot{Q} = \Omega_{\text{Axion}}^Q V, \quad \dot{U} = \Omega_{\text{Axion}}^U V, \quad \dot{V} = -\Omega_{\text{Axion}}^Q Q - \Omega_{\text{Axion}}^U U, \quad (33)$$

where

$$\Omega_{\text{Axion}}^Q = \frac{2g_{a\gamma\gamma}^2 m_a^2 \bar{k}_0 (1 - \cos \bar{\theta})^2 \bar{I}(\bar{\mathbf{p}}) \sin 2\bar{\phi}}{\left((2\bar{p}_0 \bar{k}_0 (1 - \cos \bar{\theta}) + im_a \Gamma)^2 - m_a^4 \right)}, \quad (34)$$

and

$$\Omega_{\text{Axion}}^U = \frac{2g_{a\gamma\gamma}^2 m_a^2 \bar{k}_0 (1 - \cos \bar{\theta})^2 \bar{I}(\bar{\mathbf{p}}) \cos 2\bar{\phi}}{\left((2\bar{p}_0 \bar{k}_0 (1 - \cos \bar{\theta}) + im_a \Gamma)^2 - m_a^4 \right)}. \quad (35)$$

According to Eqs. (33), linear polarization of radiation (Q and/or U \neq 0) can be converted into circular polarization depending on the evolving parameters of both the axion and the laser beams. According to our expectations, the intensity of photons does not change during the photon-photon forward scattering and only the polarization vector can change in this process. As is obvious from Eqs. (34) and (35), and owing to the smallness of $im_a \Gamma$, there is an approximate pole (resonance) at

$$s - m_a^2 = 2\bar{p}_0 \bar{k}_0 (1 - \cos \bar{\theta}) - m_a^2 \approx 0. \quad (36)$$

The resonance occurs in the s -channel of photon-photon scattering [see the first diagram in left-side of Fig. (1)] where a photon from the probe beam and one from the target create real, on shell, axions. When on-shell axions are produced, because of their very long life times, they escape the apparatus. This production of axions in light-by-light scattering is analogous to the searches for supersymmetric dark matter as "missing energy", and other long lived particle searches, at high energy colliders like the LHC. This will change the photon intensity and is not captured considering only forward scattering. Close to the resonance point, we expect a large enhancement in the conversion rate between circular and linear polarizations in the forward scattering term.

Next, we present the time evolution of Stokes parameters due to QED EH Lagrangian, treated as a competing process to the effect due to axions.

B. Circular Polarization Due to Euler-Heisenberg Lagrangian

The polarization effects caused by virtual electron-positron pairs have recently been considered taking in the quantum Boltzmann approach [50, 65]. Taking the EH Lagrangian Eq. (1), the time evolution of the density matrix given by the forward-scattering term is [44, 46, 47, 66]

$$\begin{aligned} \dot{\rho}_{ij}(\mathbf{k})^{\gamma(\text{QED})} = & -\frac{2i\alpha^2}{45m_e^4 k_0} \int \frac{d^3 p}{(2\pi)^3 2p^0} \left[g^{\mu\mu'} g^{\nu\nu'} g^{\alpha\alpha'} g^{\beta\beta'} + \frac{7}{4} \varepsilon^{\mu\nu\mu'\nu'} \varepsilon^{\alpha\beta\alpha'\beta'} \right] (\rho_{r'r'}(\mathbf{p}) + \rho_{r'r}(\mathbf{p})) (\delta_{s'i} \rho_{sj}(\mathbf{k}) - \delta_{sj} \rho_{is'}(\mathbf{k})) \\ & \times \left[(k_\mu \varepsilon_{s\nu}(k) - k_\nu \varepsilon_{s\mu}(k)) (k_{\alpha'} \varepsilon_{s'\beta'}(k) - k_{\beta'} \varepsilon_{s'\alpha'}(k)) (p_{\mu'} \varepsilon_{r\nu'}(p) - p_{\nu'} \varepsilon_{r\mu'}(p)) (p_\alpha \varepsilon_{r'\beta}(p) - p_\beta \varepsilon_{r'\alpha}(p)) \right] + \mathcal{O}(\alpha^4). \end{aligned} \quad (37)$$

Regarding our assumptions Eqs. (29)-(31), the time evolution of the Stokes parameters can be read off from Eq. (37) as

$$\dot{I} = 0, \quad \dot{Q} = \Omega_{\text{QED}}^Q V, \quad \dot{U} = \Omega_{\text{QED}}^U V, \quad \dot{V} = -\Omega_{\text{QED}}^Q Q - \Omega_{\text{QED}}^U U, \quad (38)$$

where

$$\Omega_{\text{QED}}^Q = \left(\frac{48\alpha^2 \bar{k}_0}{45m_e^4} \right) (1 - \cos \bar{\theta})^2 \bar{I}(\bar{\mathbf{p}}) \sin 2\bar{\phi}, \quad (39)$$

and

$$\Omega_{\text{QED}}^U = \left(\frac{48\alpha^2 \bar{k}_0}{45m_e^4} \right) (1 - \cos \bar{\theta})^2 \bar{I}(\bar{\mathbf{p}}) \cos 2\bar{\phi}, \quad (40)$$

Obviously, Eqs. (38) have a similar structure to Eqs. (33). These equations shows linear-to-circular polarization conversion of a light beam when it passes through a polarized vacuum, like the QED vacuum, due to vacuum birefringence. Regarding Eqs. (39) and (40), the conversion rate becomes maximum in a head-on collision of two laser beams ($\bar{\theta} = \pi$), and tends to zero when the collision angle is close to zero ($\bar{\theta} \approx 0$).

III. POLARIZATION EVOLUTION IN COLLISION OF TWO LASER BEAMS AND THE SEARCH OF AXIONS

A. Induced Ellipticity in LBL Scattering for QED and Axions

In order to probe axion fluctuations in the vacuum, we propose an experiment based on measuring the induced ellipticity on a linearly polarized probe laser beam passing through a high intensity target beam, see Fig. 2 (the situation depicted in Fig. (2) is the configuration of two incident counter-propagating laser beams inside a tunable cavity, which we will come back to later). Our physical observables in this setup are the ellipticity angle (ε) and the rotation angle of the polarization plane (ψ). The Stokes parameters may be expressed in terms of ε and ψ as [50]

$$\psi = \frac{1}{2} \arctan\left(\frac{U}{Q}\right), \quad (41)$$

$$\varepsilon = \frac{1}{2} \arcsin\left(\frac{V}{I}\right). \quad (42)$$

Ellipticity ε quantifies the relative phase between two propagating modes and ψ defines the rotation angle of the major axis of the ellipse. The set of Eqs. (33) and (38) lead to a simple harmonic equation for the circular polarization parameter V :

$$\dot{V} + \Omega^2 V = 0, \quad (43)$$

where the frequency of the oscillation Ω contains both the axion and QED contributions and is given by

$$\Omega = \Omega_{\text{Axion}} + \Omega_{\text{QED}}, \quad (44)$$

here

$$\Omega_{\text{Axion}} = \sqrt{(\Omega_{\text{Axion}}^Q)^2 + (\Omega_{\text{Axion}}^U)^2}, \quad (45)$$

and

$$\Omega_{\text{QED}} = \sqrt{(\Omega_{\text{QED}}^Q)^2 + (\Omega_{\text{QED}}^U)^2}. \quad (46)$$

The harmonic Eq. (43) implies that the generation rate of circular polarization through Faraday conversion is proportional to Ω . Supposing a totally linearly polarized probe beam in the Q direction with initial polarization values as $V_0 = 0$, $U_0 = 0$ and $Q_0 = I$, the solution of Eq. (43) is given by

$$V = -\left(\sin(2\bar{\phi}) I \right) \sin(\Omega \Delta t), \quad (47)$$

where Δt is the duration of the LBL scattering and I is the intensity of the probe laser beam. Using Eqs. (42) and Eq. (47), the absolute value of the ellipticity acquired by probe photons at a fixed azimuthal angle $\bar{\phi} = \pi/4$ is

$$\varepsilon = \frac{\Omega \Delta t}{2} = \frac{\Omega \ell}{2c}, \quad (48)$$

where ℓ is the effective length of the interaction region and c is the speed of light. Note that $\ell = 2\pi\omega_0^2/\lambda_r$ is twice the Rayleigh length, where ω_0 and λ_r are the minimum value of the beam waist and the target laser wavelength, respectively [67]. Regarding our assumed initial values for the polarization parameters and the azimuthal angle, through Eqs. (33), (38) and (41), we find that

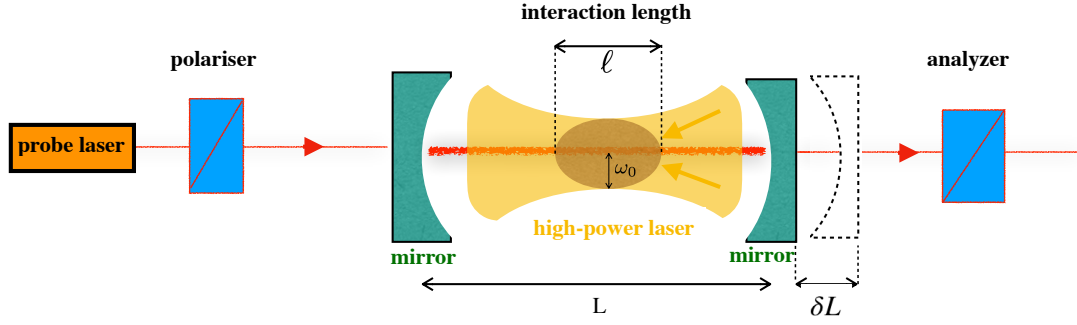


FIG. 2: Schematic setup of the laser-laser collision experiment inside a tunable cavity. A probe laser beam interacts with a high power laser which is focused into a region with a minimum beam waist ω_0 . Two incident lasers are counter-propagating and the polarization changes of the probe beam will be measured by a polarimeter outside the cavity. In this setup, laser wavelength tuning can be done by changing the cavity length.

the polarization plane ψ does not rotate during the forward scattering process. Consequently Stokes parameter $Q = I \cos(\Omega\Delta t)$ and U is identically zero.

We focus on the ellipticity signal generated in LBL as a sign of virtual axions. In our proposed experiment a high power (Peta Watt, PW, class) laser is employed to polarize the vacuum and a second laser is used to probe the vacuum structure. A linearly polarized optical, x-ray or Gamma-ray beam can be used to probe the vacuum fluctuations for both virtual axions and virtual electron-positron pairs [68–70]. Note that the probe field should be much less intense than the target laser beam. The technology of high-intensity lasers of PW class can achieve strong field strengths of the order of $10^{11} - 10^{12}G$ but limited to short spatial regions $\omega_0 = 1 - 10\mu m$, introduced by the laser pulse length [71–77]. The critical limit of intensity $I_c \simeq 4 \times 10^{29}W/cm^2$, called the Schwinger intensity, is equivalent to the critical electric (magnetic) field $E_c = 1.3 \times 10^{16}V/cm$ ($B_c = 4.4 \times 10^{13}G$) where the quantum vacuum breaks down through Schwinger pair production. Currently, high-power lasers operate in a wide range of intensities $10^{14} - 10^{23}W/cm^2$. The laser system of the Extreme Light Infrastructure for Nuclear Physics (ELI-NP) [78] and ELI-BL [79] are able to reach intensities of $10^{23}W/cm^2$, which is currently the world's most powerful laser system [80]. Upcoming facilities such as the Exawatt Center for Extreme Light Studies (XCELS) [77] envisage even higher intensities of the order of $(10^{25} - 10^{26})W/cm^2$, with a future plan to breach the 1 EW threshold [81, 82].

The total ellipticity signal generated during the LBL scattering process is $\varepsilon = \varepsilon_{QED} + \varepsilon_{Axion}$. We are looking for the ellipticity signal originating from *off-shell* axions on top of the QED background, as well as several different noise sources. While the Standard Model LBL scattering with low energy photons has never been observed so far, here we are interested in removing QED effects, leaving behind only axions signal.

The ratio of the ellipticity signal generated in LBL by exchanging relatively heavy ($m_a \gg \omega$) off-shell axions to the signal originating from QED processes is given by

$$\frac{\varepsilon_{Axion}}{\varepsilon_{QED}} = \frac{\Omega_{Axion}^{(m_a^2 \gg s)}}{\Omega_{QED}} = 1.87 \times \left(\frac{m_e}{m_a}\right)^2 \left(\frac{g_{a\gamma\gamma} m_e}{\alpha}\right)^2. \quad (49)$$

In order for the ALP contribution to be dominant, $g_{a\gamma\gamma}/m_a$ should satisfy the following condition

$$\left(\frac{g_{a\gamma\gamma}}{m_a}\right)_{ALPs} \gtrsim 0.73 \times \left(\frac{\alpha}{m_e^2}\right) = \frac{2.05 \times 10^{-5}}{(eV)(GeV)}. \quad (50)$$

For low energy photons in the range of radio or microwave frequencies, the effect of ALP induced polarization fluctuation in vacuum surpasses the QED effect due to electron-positron pairs for $m_a \approx \mu eV$ if $g_{a\gamma\gamma} \gtrsim 2.05 \times 10^{-11}(GeV)^{-1}$, and for $m_a \approx meV$ if $g_{a\gamma\gamma} \gtrsim 2.05 \times 10^{-8}(GeV)^{-1}$. For the case of the QCD axions, using Eqs. (18) and (19), $g_{a\gamma\gamma}/m_a$ is obtained as

$$\left(\frac{g_{a\gamma\gamma}}{m_a}\right)_{QCD} \approx \frac{1.93 \times 10^{-10}}{(eV)(GeV)}. \quad (51)$$

However, for the axion masses comparable to the photon energies and close to resonance, one cannot simply integrate out the axionic degrees of freedom. In this case the signal is enhanced further, and a larger part of the parameter space has axion effects dominant over those from QED.

In the next section we take realistic experimental parameters capable to measure the induced ellipticity signal in high power laser experiments and compute the sensitivity to axion induced polarization evolution.

B. Sensitivity to Axion Parameters

In order to evaluate the axion contribution to the ellipticity signal we take Eqs. (34), (35), (45) and (48). Detection of the ellipticity seems to be more feasible near the resonance region (Eq. 36), where we expect a large enhancement in the signal. The signal enhancement near the resonance can be applied in order to discriminate between the axion contribution to photon-photon scattering and the one originating from QED. In fact, the ellipticity signal is a function of the axion-photon coupling and the axion mass, so a precise measurement of the ellipticity can put an upper bound on these parameters if a signal is not observed.

Since $m_a \Gamma_a$ is sufficiently small with respect to m_a^2 and $s = 2\bar{p} \cdot \bar{k}$, we find ϵ_{Axion} is given by

$$\epsilon_{\text{Axion}} = g_{a\gamma\gamma} m_a^2 \bar{k}_0 \frac{(1 - \cos \bar{\theta})^2}{s^2 - m_a^4} \frac{\bar{I}(\bar{\mathbf{p}}) \ell}{c} \quad (52)$$

In addition to the axion parameters, the ellipticity signal depends on the energy of the photons in the colliding beams, the intensity of the target beam, the interaction length, and the collision angle between the two lasers. In the case of relatively light axions with respect to the photon energy, $s \gg m_a^2$, we can approximate ϵ_{Axion} as

$$\epsilon_{\text{Axion}}^{(s \gg m_a^2)} = \left(\frac{g_{a\gamma\gamma} m_a^2 \ell}{4\bar{p}_0^2 \bar{k}_0 c} \right) \bar{I}(\bar{\mathbf{p}}) = 7.91 \times 10^{-10} \text{rad} \left(\frac{g_{a\gamma\gamma}}{10^{-6} \text{GeV}^{-1}} \right)^2 \left(\frac{m_a}{\text{eV}} \right)^2 \left(\frac{\text{eV}}{\bar{p}_0} \right)^2 \left(\frac{\text{eV}}{\bar{k}_0} \right) \left(\frac{\bar{I}(\bar{\mathbf{p}})}{10^{23} \text{W/cm}^2} \right) \left(\frac{\ell}{100 \mu\text{m}} \right). \quad (53)$$

Since the axion is a pseudoscalar, this has no angular dependence, which gives a peculiar signature of virtual axions. In contrast to light axions, the ellipticity receives no contribution from QED processes when the probe beam is aligned along with the target laser beam ($\bar{\theta} \approx 0$). This provides an ideal situation in order to isolate polarization features stemming only from axions. We propose to use an optical probe laser beam with $\bar{k}_0 \sim 1.5$ eV crossing another laser beam with an intensity of the order of 10^{23}W/cm^2 and an energy per light quantum $\bar{p}_0 \sim 1$ eV focused to a region with $\omega_0 \sim 10 \mu\text{m}$ or equivalently $\ell \sim 507 \mu\text{m}$. A negative result of the ellipticity measurements applying high precision polarimeters with resolution down to 10^{-10} rad leads to the following forecasted constraint on the axion parameters

$$\left(\frac{g_{a\gamma\gamma}}{\text{GeV}^{-1}} \right) \left(\frac{m_a}{\text{eV}} \right) \lesssim 1.93 \times 10^{-7}. \quad (54)$$

Taking $\bar{I}(\bar{\mathbf{p}}) \sim 10^{25} \text{W/cm}^2$ as the highest intensity which is envisaged to be available at the ELI and at XCELS, the upper limit would be improved to 1.93×10^{-8} . It is worth noting that measurement of the ellipticities of the order of 10^{-10} rad has already been reported in the optical regime [24, 83]. The detection sensitivity of the ellipsometer is limited by both shot noise and the light source stability. However, the large number of probe photons ($\sim 10^{20}$) provided by high power laser systems such as ELI and XCELS are sufficient to put strong constraints on axion parameters.

For those axions which are heavier than the typical energy scale of incident photons ($m_a^2 \gg s$), the ellipticity angle generated in LBL scattering can be approximated as

$$\epsilon_{\text{Axion}}^{(m_a^2 \gg s)} = 3.16 \times 10^{-9} \text{rad} (1 - \cos \bar{\theta})^2 \left(\frac{g_{a\gamma\gamma}}{10^{-6} \text{GeV}^{-1}} \right)^2 \left(\frac{\text{eV}}{m_a} \right)^2 \left(\frac{\bar{k}_0}{\text{eV}} \right) \left(\frac{\bar{I}(\bar{\mathbf{p}})}{10^{23} \text{W/cm}^2} \right) \left(\frac{\ell}{100 \mu\text{m}} \right). \quad (55)$$

which is inversely proportional to the squared mass of axions, so by increasing m_a the ellipticity angle will be decreased.

In the region close to the resonance point where $s \simeq m_a^2$, the induced ellipticity on the probe beam is

$$\epsilon_{\text{Axion}}^{(s \simeq m_a^2)} = 1.58 \times 10^{-9} \frac{(1 - \cos \bar{\theta})^2}{\epsilon} \left(\frac{g_{a\gamma\gamma}}{10^{-6} \text{GeV}^{-1}} \right)^2 \left(\frac{\text{eV}}{m_a} \right)^2 \left(\frac{\bar{k}_0}{\text{eV}} \right) \left(\frac{\bar{I}(\bar{\mathbf{p}})}{10^{23} \text{W/cm}^2} \right) \left(\frac{\ell}{100 \mu\text{m}} \right), \quad (56)$$

where ϵ is defined as a small deviation from the resonance, $s = m_a^2 + \epsilon m_a^2$ and $\frac{\Gamma}{m_a} \leq \epsilon \ll 1$. Moreover we can rewrite ϵ as follows

$$\epsilon = \frac{2\bar{p}_0 \bar{k}_0}{m_a^2} (1 - \cos \bar{\theta}) - 1. \quad (57)$$

for those values of ϵ which are close enough to zero the generation rate of circular polarization can be substantially enhanced. The enhancement of the polarization signal occurs at some special angles defined by

$$\theta = \cos^{-1} \left[1 - \frac{m_a^2}{2\bar{p}_0 \bar{k}_0} \right]. \quad (58)$$

We note again that the resonant enhancement is absent in the competing QED process and can be used as a specific signature of axions.

We rewrite Eq. (56) near the resonance point $2\bar{p}^0\bar{k}^0(1 - \cos\bar{\theta}) \approx m_a^2$ as follows

$$\varepsilon_{\text{Axion}}^{(s \approx m_a^2)} = \frac{7.9 \times 10^{-10}}{\varepsilon} (1 - \cos\bar{\theta}) \left(\frac{g_{a\gamma\gamma}}{10^{-6} \text{GeV}^{-1}} \right)^2 \left(\frac{eV}{\bar{p}_0} \right) \left(\frac{\bar{I}(\bar{\mathbf{p}})}{10^{23} \text{W/cm}^2} \right) \left(\frac{\ell}{100 \mu\text{m}} \right). \quad (59)$$

Thus by fixing the energies of both the probe and the target laser beams (e.g. \bar{k}_0 and \bar{p}_0), and looking for the ellipticity enhancement at different angles, one may determine the mass of the axion: the collision angle scans the resonance. Furthermore the amplitude of the signal gives an measurement of $g_{a\gamma\gamma}$. Instead of changing the collision angle, one can also scan the resonance using a tunable cavity [See Fig. 2], where now the collision angle is fixed and the energy of the probe photons varies inside the cavity. In this setup, wavelength tuning is achieved by variation of the cavity length or by alternative tuning mechanisms. Applying a Fabry-Perot cavity with length L and finesse \mathcal{F} leads to cavity modes which are separated by free spectral range (FSR) $\omega_{fsr} = \pi c/L$ where

$$\omega_{fsr} = 6.19 \times 10^{-5} \text{eV} \left(\frac{\text{cm}}{L} \right). \quad (60)$$

The width of the cavity modes is determined by the finesse as $\Delta\omega_c = \omega_{fsr}/\mathcal{F}$ [84]. Using high finesse cavities let us probe different mass ranges with incredible precision. While a short high power pulse interacting with a probe laser beam along with the interaction length ℓ [Fig. 2], the energy of the probe photons would change in FSR steps in order to scan over a finite mass range of axions.

For the resonance frequency $\bar{k}^0 \approx m_a^2/4\bar{p}^0$ in a two-beam head-to-head collision, cavity length needs to be changed by $\delta L \sim 1/2\bar{k}^0$ in order to continuously scan this frequency range by using different cavity modes [84]. In order to probe a limited mass range $10^{-2} \text{eV} \lesssim m_a \lesssim 1 \text{eV}$ in a reasonable time scale (≈ 1 year), we propose to use a cavity length $L = 62 \text{cm}$ ($\omega_{fsr} \approx 10^{-6} \text{eV}$) which implies $\Delta\omega_c = 10^{-11} \text{eV}$ with cavity finesse $\mathcal{F} \sim 10^5$. This leads to $\varepsilon \approx 10^{-11}$ as the enhancement factor on resonance. The induced ellipticity for input parameters $\bar{I}(\bar{\mathbf{p}}) = 10^{25} \text{W/cm}^2$, $\bar{p}_0 \sim 1 \text{eV}$, $\ell \sim 507 \mu\text{m}$ and $(\bar{\theta} \approx \pi)$ is given by

$$\varepsilon_{\text{Axion}} = 8.01 \times 10^{16} \left(\frac{g_{a\gamma\gamma}}{\text{GeV}^{-1}} \right)^2, \quad (61)$$

where the resonance condition fixed the axion mass at $m_a \approx 2\sqrt{\bar{k}^0}$. The current accuracy of ellipticity measurements of about 10^{-10} rad is sufficient to put an upper bound $3.5 \times 10^{-14} \text{GeV}^{-1}$ on the axion-photon coupling $g_{a\gamma\gamma}$. The ellipsometry resolution 10^{-10} is only accessible for high power laser beams with a large number of photons ($\sim 10^{20}$). However, recently it has been claimed that high precision phase measurements are also possible using lower power lasers in squeezed state [67].

In our proposed experiment the monochromaticity of the probe beam is essential for scanning the resonance mass, and in order to have an ideal monochromatic laser beam an infinite pulse length is required. However, high power lasers usually have short pulse duration $\tau \approx \mathcal{O}(10 - 100) \text{fs}$. A typical pulse length larger than the oscillation of the laser beam serve as a good approximation for monochromatic light [23]. For high power lasers in optical frequencies $\bar{k}_0 \approx 1 \text{eV}$ and for pulse duration $10^{-14} - 10^{-11} \text{s}$, one would obtain $\Delta\bar{k}/\bar{k}_0 \approx 10^{-2} - 10^{-5}$. The lowest bandwidth for continuous-wave (CW) low-power lasers such as He-Ne laser is about 1.5 GHz. A very narrow bandwidth down to 1 kHz or even less is obtainable by applying stabilized low-power CW lasers. Note that the observed bandwidth is limited by fundamental quantum processes and technical noise.

Instead of polarimetry, one may use interferometric techniques in order to measure a phase shift introduced by axions on the probe photons. Recently it was proposed to set a Mach-Zehnder interferometer (MZI) to measure a very small phase shift between a probe beam passed through a disturbed quantum vacuum and the same beam propagated in an unperturbed vacuum [67]. The theoretical bound for the phase sensitivity measurement when a coherent classical light is applied is $\sim 1/\sqrt{\langle N \rangle}$ where $\langle N \rangle$ is the average number of photons. Squeezed state of light can improve the phase sensitivity of an interferometer reaching to $\sim 1/\langle N \rangle$. While for a classical light a large number of photons is needed to obtain high sensitivity in phase measurement, a CW laser in the squeezed state can achieve the same sensitivity but with smaller number of photons.

Note that for a polarization analyzer the quantity $1/\sqrt{aI_0\tau\eta}$ is the amplitude of shot noise [85], where I_0 is the incident photon flux to analyzer, a is the light-extinction ratio of the polarization analyzer, τ is the photon counting time and η is the quantum efficiency of the photodetector.

In order to avoid background noise in the presence of charged particles such as the Cotton-Mouton and Kerr effects [86], it is essential to completely clean the interaction region by eliminating all residual gas particles from the interaction region [87]. Apart from this background noise, we demand that the axion ellipticity signal surpasses the similar signal produced by QED process. Taking into account Eqs. (39), (40), (46), and (48) the induced ellipticity ε_{QED} on a probe laser beam is given by

$$\varepsilon_{\text{QED}} = \left(\frac{48\alpha^2\bar{k}_0L}{90m_e^4c} \right) (1 - \cos\bar{\theta})^2 \bar{I}(\bar{\mathbf{p}}) = 1.32 \times 10^{-6} \text{rad} (1 - \cos\bar{\theta})^2 \left(\frac{\bar{k}_0}{\text{eV}} \right) \left(\frac{\bar{I}(\bar{\mathbf{p}})}{10^{23} \text{W/cm}^2} \right) \left(\frac{\ell}{100 \mu\text{m}} \right). \quad (62)$$

Keeping the same experimental parameters as those used in order to compute Eq. (61) namely $\bar{I}(\bar{\mathbf{p}}) = 10^{25} \text{W/cm}^2$, $\ell \sim 507 \mu\text{m}$ and $\bar{\theta} = \pi$, this quantity can be evaluated as $\varepsilon_{\text{QED}} = 2.67 \times (10^{-8} - 10^{-3}) \text{rad}$ for $\bar{k}_0 \sim 10^{-5} - 1 \text{eV}$. Taking the QED signal

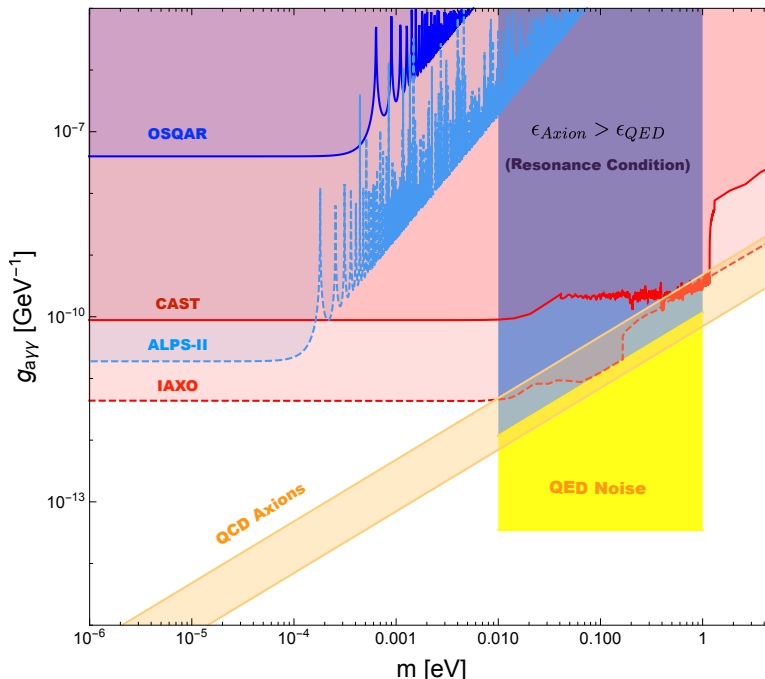


FIG. 3: Exclusion regions in the $(g_{a\gamma\gamma}, m_a)$ -plane obtained from the discovery potential of our proposed experiment using high-power lasers. We assume a linearly polarized laser beam counter-propagating along with a high-power laser [Fig. 2] which satisfies the resonance condition Eq. (61) in the mass range $10^{-2}\text{eV} \lesssim m_a \lesssim 1\text{eV}$, taking into account high-precision polarimeters. The dark blue region as labeled shows the region in which the axion ellipticity signal is larger than QED ellipticity signal with accuracy up to 3σ . The light yellow part could result from ellipticity measurement with accuracy 10^{-10} rad of a probe laser beam interacting with a high power laser $10^{25}\text{W}/\text{cm}^2$ close to the resonance points, but the signal lies below the QED background.

as a background noise, the sensitivity $g_{a\gamma\gamma} \gtrsim 1.58 \times (10^{-12} - 10^{-10})\text{GeV}^{-1}$ is obtained from the signal to noise ratio (SNR), $\text{SNR} = 3$ for the resonance mass range $10^{-2}\text{eV} \lesssim m_a \lesssim 1\text{eV}$. This is illustrated in Fig. (3), which represents the sensitivity of our proposed set up to axion parameters. The dark blue region is where the axion ellipticity signal is well above the QED ellipticity signal, with accuracy up to 3σ . The light yellow region is the region in which axion signal is observable according to sensitivity of our polarimeter, but below the QED noise. In the yellow region, the axion signal could in principle be measured as an addition to the QED signal, but this would require more careful analysis.

IV. CONCLUSION AND REMARKS

In the present paper we have considered the polarization features originating from virtual axion exchange in the photon-photon scattering process. Our adopted formalism is based on the quantum Boltzmann equation, which gives the time evolution of the Stokes parameters. This formalism presents more details compared with the previous semi-classical approaches and reveals some new features such as the resonance pole of axions. One of the advantages of the polarization analysis in the forward scattering with respect to many other experiments is that the former relies on the scattering amplitude $\sqrt{\sigma_{\gamma\gamma}}$ instead of scattering cross section $\sigma_{\gamma\gamma}$. In Light-Shining through Wall (LSW) experiments, real axions are produced and the observational signal is proportional to $g_{a\gamma\gamma}^4$ [88, 89], whereas our polarization signal scales as $g_{a\gamma\gamma}^2$ for axion masses sufficiently far from the resonance. However, close to the resonance point, the polarization signal enhances as $g_{a\gamma\gamma}^2/\epsilon$, where ϵ is limited by the bandwidth of the probe laser beam and can be as small as 10^{-11} .

We used parameters of existing high power laser designs in order to constrain axion parameters. The effect of axions producing an elliptical polarization signal for an initially linear polarized optical probe laser beam was investigated, during the interaction with an ultrahigh intensity laser background. We then compared the generated ellipticity signal in different ranges of axion parameters with the corresponding polarization signals caused by nonlinear QED effects. It was shown that the ellipticity signal increases as a function of the average intensity of the target laser beam, the interaction length of two lasers, and also the energy of the probe photons. Our proposed experiment appears to have sufficient sensitivity to span considerable range of axion masses

$10^{-2}eV \lesssim m_a \lesssim 1eV$. The potential discovery reach of this experimental setup is summarized in Fig. (3). Remarkably, we show that our scheme can explore a broad range of axion masses reaching the QCD axion parameter region while remaining above the QED background at 3σ . Our results thus show the unique potential of light-by-light scattering to probe axions, and it can become a valuable complement to other studies to determine axion parameters and shedding light on the nature of the axion-photon interaction.

Acknowledgements

S. S would like to thank R. Mohammadi for collaboration at the early stages of this project. S. S would like to thank M. Zarei and M. Abdi for many fruitful discussions, he is also grateful to Georg-August Universität of Göttingen and ICRANet head quarter in Pescara for kind hospitality when this work was in progress. DJEM is supported by the Alexander von Humboldt Foundation and the German Federal Ministry of Education and Research.

-
- [1] R. D. Peccei and H. R. Quinn, *Physical Review Letters* **38**, 1440 (1977).
 - [2] S. Weinberg, *Phys. Rev. Lett.* **40**, 223 (1978).
 - [3] F. Wilczek, *Phys. Rev. Lett.* **58**, 1799 (1987).
 - [4] S.-J. Chen, H.-H. Mei, and W.-T. Ni, *Modern Physics Letters A* **22**, 2815 (2007), hep-ex/0611050.
 - [5] P. Svrcek and E. Witten, *JHEP* **06**, 051 (2006), hep-th/0605206.
 - [6] A. Arvanitaki, S. Dimopoulos, S. Dubovsky, N. Kaloper, and J. March-Russell, *Phys. Rev.* **D81**, 123530 (2010), 0905.4720.
 - [7] L. F. Abbott and P. Sikivie, *Phys. Lett.* **120B**, 133 (1983).
 - [8] M. Dine and W. Fischler, *Phys. Lett.* **120B**, 137 (1983).
 - [9] J. Preskill, M. B. Wise, and F. Wilczek, *Phys. Lett.* **120B**, 127 (1983).
 - [10] V. Anastassopoulos, S. Aune, K. Barth, A. Belov, H. Bräuninger, G. Cantatore, J. M. Carmona, J. F. Castel, S. A. Cetin, F. Christensen, et al., *Nature Physics* **13**, 584 (2017), 1705.02290.
 - [11] P. Sikivie, *Phys. Rev. Lett.* **51**, 1415 (1983).
 - [12] P. Sikivie, *Phys. Rev. D* **32**, 2988 (1985).
 - [13] J. Hoskins, J. Hwang, C. Martin, P. Sikivie, N. S. Sullivan, D. B. Tanner, M. Hotz, L. J. Rosenberg, G. Rybka, A. Wagner, et al., *Phys. Rev. D* **84**, 121302 (2011).
 - [14] S. Asztalos, E. Daw, H. Peng, L. J. Rosenberg, C. Hagmann, D. Kinion, W. Stoeffl, K. van Bibber, P. Sikivie, N. S. Sullivan, et al., *Phys. Rev. D* **64**, 092003 (2001).
 - [15] I. Obata, T. Fujita, and Y. Michimura, *Physical Review Letters* **121**, 161301 (2018), 1805.11753.
 - [16] H. Liu, B. D. Elwood, M. Evans, and J. Thaler, arXiv e-prints (2018), 1809.01656.
 - [17] Y. Michimura, N. Matsumoto, N. Ohmae, W. Kokuyama, Y. Aso, M. Ando, and K. Tsubono, *Physical Review Letters* **110**, 200401 (2013), 1303.6709.
 - [18] D. Espriu and A. Renau, *Phys. Rev.* **D85**, 025010 (2012), 1106.1662.
 - [19] T. Liu, G. Smoot, and Y. Zhao (2019), 1901.10981.
 - [20] R. Cameron, G. Cantatore, A. C. Melissinos, G. Ruoso, Y. Semertzidis, H. J. Halama, D. M. Lazarus, A. G. Prodell, F. Nezirick, C. Rizzo, et al., *Phys. Rev. D* **47**, 3707 (1993).
 - [21] E. Zavattini, G. Zavattini, G. Ruoso, G. Raiteri, E. Polacco, E. Milotti, V. Lozza, M. Karuza, U. Gastaldi, G. Di Domenico, et al. (PVLAS Collaboration), *Phys. Rev. D* **77**, 032006 (2008).
 - [22] R. Battesti, B. Pinto da Souza, S. Batut, C. Robilliard, G. Bailly, C. Michel, M. Nardone, L. Pinard, O. Portugall, G. TraNec, et al., *European Physical Journal D* **46**, 323 (2008), 0710.1703.
 - [23] S. Villalba-Chavez, *Nuclear Physics B* **881**, 391 (2014), 1308.4033.
 - [24] S. Villalba-Chávez and A. Di Piazza, *Journal of High Energy Physics* **11**, 136 (2013), 1307.7935.
 - [25] D. Bernard, in *Nuclear Physics B Proceedings Supplements* (LPNHE, Ecole Polytechnique, IN2P3 & CNRS, 91128 Palaiseau, France, 1999), pp. 201–205.
 - [26] F. Moulin, D. Bernard, and F. Amiranoff, *Z. Phys.* **C72**, 607 (1996).
 - [27] E. Massó and R. Toldrà, *prd* **52**, 1755 (1995), hep-ph/9503293.
 - [28] S. Evans and J. Rafelski, *Phys. Lett.* **B791**, 331 (2019), 1810.06717.
 - [29] Z. Bogorad, A. Hook, Y. Kahn, and Y. Soreq (2019), 1902.01418.
 - [30] H. Euler, *Annalen der Physik* **418**, 398 (1936).
 - [31] W. Heisenberg and H. Euler, *Zeitschrift für Physik* **98**, 714 (1936).
 - [32] D. A. Dicus, C. Kao, and W. W. Repko, *Physical Review D (Particles)* **57**, 2443 (1998).
 - [33] G. V. Dunne, *International Journal of Modern Physics A* **27**, 1260004 (2012), 1202.1557.
 - [34] J. Schwinger, *Physical Review* **82**, 664 (1951).
 - [35] S. Knapen, T. Lin, H. Keong Lou, and T. Melia, ArXiv e-prints (2017), 1709.07110.
 - [36] C. Baldenegro, S. Hassani, C. Royon, and L. Schoeffel (2019), 1903.04151.

- [37] M. Aaboud, G. Aad, B. Abbott, J. Abdallah, O. Abidinov, B. Abeloos, S. H. Abidi, O. S. Abouzeid, N. L. Abraham, H. Abramowicz, et al., *Nature Physics* **13**, 852 (2017), 1702.01625.
- [38] M. Klusek-Gawenda, P. Lebedowicz, and A. Szczurek, *Phys. Rev. C* **93**, 044907 (2016), 1601.07001.
- [39] D. d'Enterria and G. G. da Silveira, *Physical Review Letters* **111**, 080405 (2013), 1305.7142.
- [40] S. Knapen, T. Lin, H. K. Lou, and T. Melia, *Physical Review Letters* **118**, 171801 (2017), 1607.06083.
- [41] C. Baldenegro, S. Fichet, G. von Gersdorff, and C. Royon, *ArXiv e-prints* (2018), 1803.10835.
- [42] L. Maiani, R. Petronzio, and E. Zavattini, *Phys. Lett.* **B175**, 359 (1986).
- [43] G. Raffelt and L. Stodolsky, *Phys. Rev.* **D37**, 1237 (1988).
- [44] S. Shakeri, S. Z. Kalantari, and S.-S. Xue, *Phys. Rev. A* **95**, 012108 (2017), 1703.10965.
- [45] M. Zarei, S. Shakeri, M. Abdi, D. J. E. Marsh, and S. Matarrese (2019), 1910.09973.
- [46] R. Mohammadi, I. Motie, and S.-S. Xue, *Phys. Rev. A* **89**, 062111 (2014), 1402.5999.
- [47] S. Shakeri, M. Haghghat, and S.-S. Xue, *Journal of Cosmology and Astroparticle Physics* **2017**, 014 (2017).
- [48] Kosowsky, A, *Ann. Phys. (USA)* **246**, 49 (1996).
- [49] Alexander, Stephon, Ochoa, Joseph, and Kosowsky, Arthur, *Physical Review D* **79**, 063524 (2009).
- [50] S. Shakeri, S. Z. Kalantari, and S.-S. Xue, *Phys. Rev.* **A95**, 012108 (2017), 1703.10965.
- [51] G. G. Raffelt, *physrep* **198**, 1 (1990).
- [52] G. G. Raffelt, *Stars as laboratories for fundamental physics* (1996), ISBN 9780226702728.
- [53] N. V. Mikheev, A. Y. Parkhomenko, and L. A. Vassilevskaya, *Phys. Rev. D* **60**, 035001 (1999), hep-ph/9903415.
- [54] N. V. Mikheev, A. Y. Parkhomenko, and L. A. Vassilevskaya, *Physics of Atomic Nuclei* **63**, 1046 (2000).
- [55] S. Weinberg, *Phys. Rev. Lett.* **40**, 223 (1978).
- [56] F. Wilczek, *Phys. Rev. Lett.* **40**, 279 (1978).
- [57] G. G. Raffelt, *J. Phys.* **A40**, 6607 (2007), hep-ph/0611118.
- [58] J. E. Kim, *Phys. Rept.* **150**, 1 (1987).
- [59] J. E. Kim, *Phys. Rev. Lett.* **43**, 103 (1979).
- [60] M. A. Shifman, A. I. Vainshtein, and V. I. Zakharov, *Nuclear Physics B* **166**, 493 (1980).
- [61] A. Zhitnitsky, *Sov. J. Nucl. Phys.* **31**, 260 (1980).
- [62] M. Dine, W. Fischler, and M. Srednicki, *Phys. Lett. B* **104**, 199 (1981).
- [63] D. Cadamuro, S. Hannestad, G. Raffelt, and J. Redondo, *jcap* **2**, 003 (2011), 1011.3694.
- [64] M. Bauer, M. Heiles, M. Neubert, and A. Thamm, *Eur. Phys. J.* **C79**, 74 (2019), 1808.10323.
- [65] S. Shakeri, M. Haghghat, and S.-S. Xue, *JCAP* **1710**, 014 (2017), 1704.04750.
- [66] S. Batebi, R. Mohammadi, R. Ruffini, S. Tizchang, and S. S. Xue, *Phys. Rev.* **D94**, 065033 (2016), 1610.01154.
- [67] S. Ataman, *Phys. Rev.* **A97**, 063811 (2018), 1807.11299.
- [68] Y. Nakamiya, K. Homma, T. Moritaka, and K. Seto, *Phys. Rev.* **D96**, 053002 (2017), 1512.00636.
- [69] S. Bragin, S. Meuren, C. H. Keitel, and A. Di Piazza, *Phys. Rev. Lett.* **119**, 250403 (2017), 1704.05234.
- [70] F. Karbstein, *Phys. Rev.* **D98**, 056010 (2018), 1807.03302.
- [71] B. King and C. H. Keitel, *New J. Phys.* **14**, 103002 (2012), 1202.3339.
- [72] A. di Piazza, C. Müller, K. Z. Hatsagortsyan, and C. H. Keitel, *Reviews of Modern Physics* **84**, 1177 (2012).
- [73] T. Heinzl and A. Ilderton, *arXiv.org* (2008), 0809.3348.
- [74] H. Gies, *The European Physical Journal D* **55**, 311 (2009).
- [75] T. Heinzl and A. Ilderton, *European Physical Journal D* **55**, 359 (2009), 0811.1960.
- [76] Hibef website, URL <http://www.hzdr.de/hibef>.
- [77] Eli, URL <http://www.hzdr.de/hibef>, "HiPER", <http://www.hiperlaser.org>, "XCELS", <http://www.xcels.iapras.ru/img/XCELS-Project-english-version.pdf>.
- [78] The website of eli-np, URL <http://www.eli-np.ro/>.
- [79] Eli beamlines petawatt lasers, URL <https://www.eli-beams.eu/>.
- [80] The extreme light infrastructure (eli) project, URL <https://eli-laser.eu>.
- [81] G. A. Mourou, N. J. Fisch, V. M. Malkin, Z. Toroker, E. A. Khazanov, A. M. Sergeev, T. Tajima, and B. Le Garrec, *Optics Communications* **285**, 720 (2012), 1108.2116.
- [82] C. Danson, D. Hillier, N. Hopps, and D. Neely, *High Power Laser Science and Engineering* **3**, e3 (2015).
- [83] K. Muroo, N. Ninomiya, M. Yoshino, and Y. Takubo, *J. Opt. Soc. Am. B* **20**, 2249 (2003).
- [84] A. C. Melissinos, *Phys. Rev. Lett.* **102**, 202001 (2009), 0807.1092.
- [85] K. Muroo, M. Namikawa, and Y. Takubo, *Measurement Science and Technology* **11**, 32 (1999).
- [86] C. Rizzo, A. Rizzo, and D. M. Bishop, *International Reviews in Physical Chemistry* **16**, 81 (2010).
- [87] H.-P. Schlenvoigt, T. Heinzl, U. Schramm, T. E. Cowan, and R. Sauerbrey, *Physica Scripta* **91**, 023010 (2016).
- [88] B. Dobrich (ALPS-II), in *Proceedings, 9th Patras Workshop (2013): Mainz, Germany, June 24-28, 2013* (2013), pp. 55–58, 1309.3965.
- [89] J. Redondo and A. Ringwald, *Contemp. Phys.* **52**, 211 (2011), 1011.3741.